Miller Range 090034, 090070, 090075

Anorthositic regolith breccia

195.57, 137.46, 143.52 g

Figure 1: *MIL 090034 (left), and MIL 090070 and MIL090075 (right) as recovered in the field. Field photo image(s) courtesy of the* ***ANSMET*** *Program, Case Western Reserve Univ. and the Univ. of Utah.*

Introduction: The 2009-10 season ANSMET team recovered MIL 090034, MIL 090070, and MIL 090075 which were classified as lunar anorthositic breccias (**Figure 1**) and reported in the Antarctic Meteorite Newsletter 33 no. 2 (Satterwhite and Righter, 2010). MIL 090034 was found in the middle Icefield area of the Miller Range, near MIL 07006 and MIL 090036, while MIL 090070 and MIL 090075 were found in the northern icefield and found just a few cm away from each other and obviously originally a single piece (**Figures 1,2**). Cosmic ray exposure age data for MIL 090034, MIL 090070, and MIL 090075 are consistent with the three being paired (Nishiizumi and Caffee, 2013), even with the ~12 km distance between the find locations. Petrographic and other information supports this pairing as will be discussed below.

Petrography and Mineralogy: MIL 090034, 090070, and 090075 are anorthositic regolith breccias with a fine-grained to glassy matrix, and clasts that range from <0.1 mm up to 3 mm in size (**Figures 3 to 7**). The clasts are dominated by impact melt breccias most of which are clast-bearing. Several coarser igneous textured rock clasts have also been documented in these three samples (Calzada-Diaz et al., 2016; Martin et al., 2017). The matrix of these samples also contains mineral fragments and clasts of plagioclase and pyroxene (Calzada-Diaz et al., 2016). (**Figures 8 to 10**).

Pyroxene and olivine Fe/Mn ratios fall as expected along a line defined by lunar samples, distinct from terrestrial or martian olivine and pyroxene (**Fig. 11**). The clasts from MIL 090034, 090070, and 090075 have a wide range of pyroxene compositions from En_{50} to En_{80}, olivine from Fo_{20} to Fo_{40}, and plagioclase An_{95} or higher (**Fig. 12-14**). The anorthositic clasts include norite and ferroan anorthosites, but there are a few gabbroic clasts with even more ferroan pyroxenes (**Fig. 13**). Consideration of both feldspar and pyroxene compositions demonstrate the affinity of the

feldspathic clasts for ferroan anorthosite (FAN) materials such as those defined in Apollo 16 samples (**Fig. 14**).

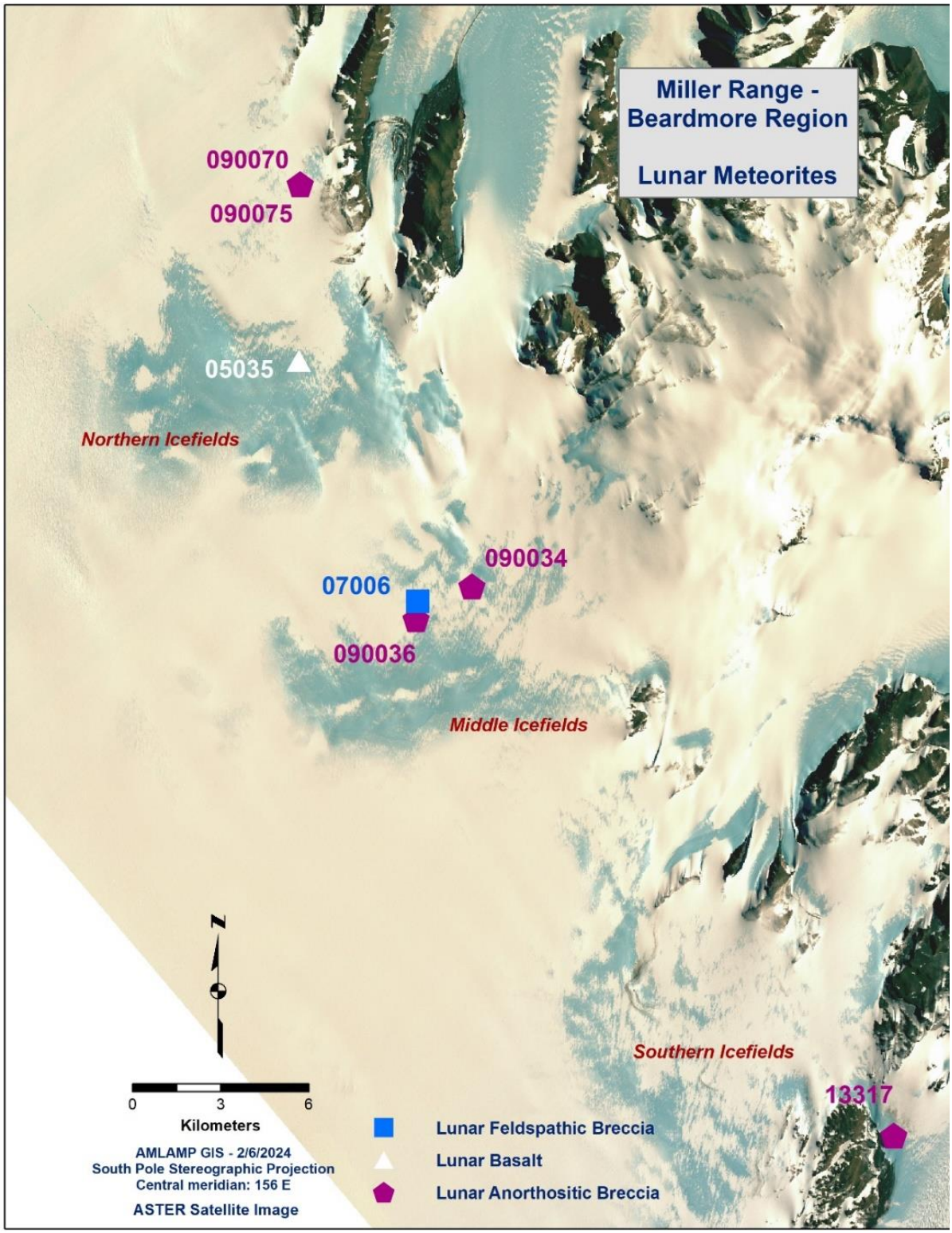

Figure 2: *Location of MIL 090034, MIL 090070, and MIL 090075 lunar meteorites from the Miller Range 2009-10 ANSMET season, in the middle and north icefields of the Miller Range (purple pentagons).*


MIL 090034,0
5/18/10

MIL 090034,0
5/18/10

MIL 090034,0
5/18/10

MIL 090034,0
5/18/10

MIL 090034,0
5/18/10

MIL 090034,0
5/18/10

MIL 090070,0
5/18/10

MIL 090070,0
5/18/10

MIL 090070,0
5/18/10

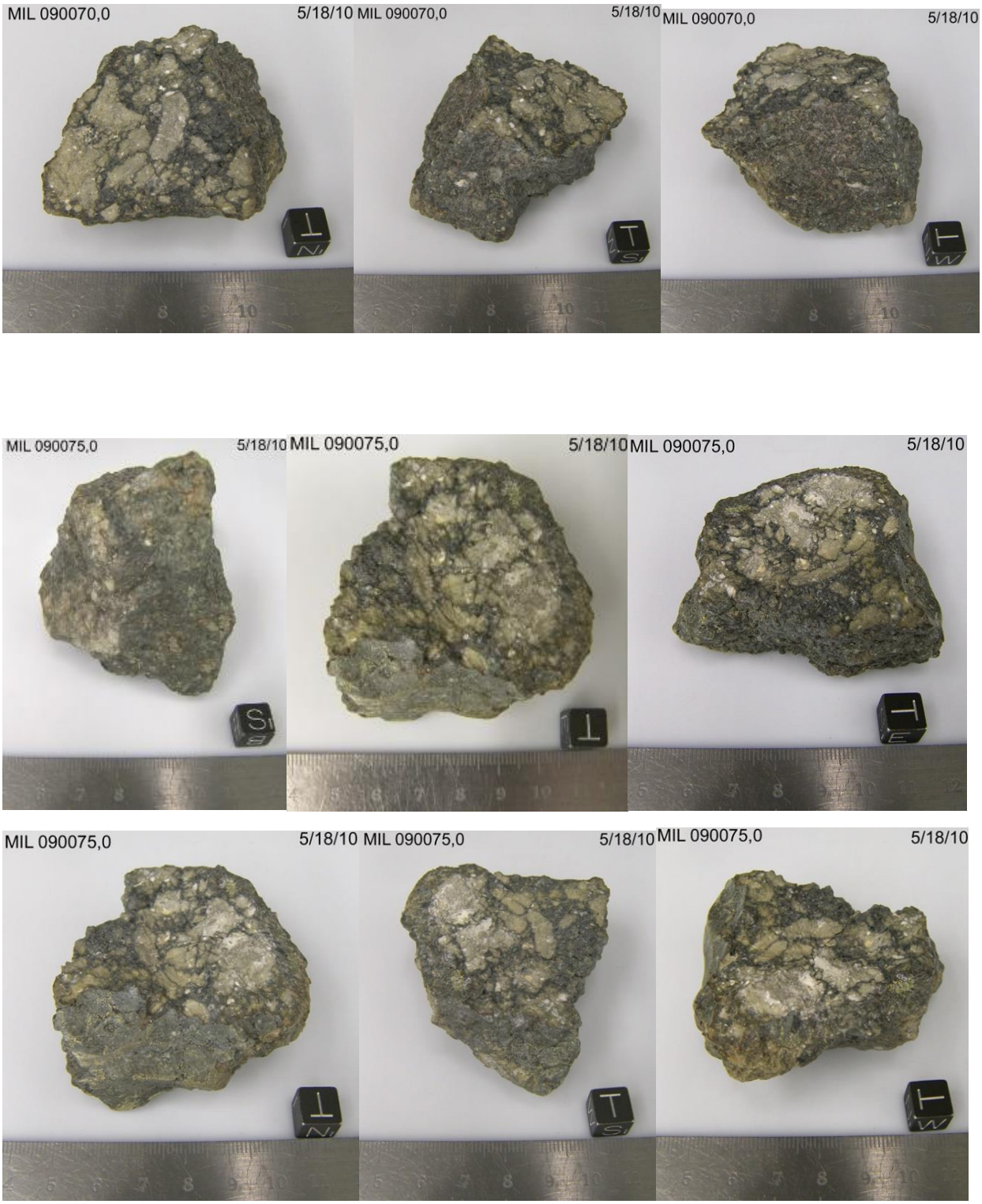

Figure 3: *Orthogonal views of lunar meteorites MIL 090034, MIL 090070, and MIL 090075, illustrating the range of clast sizes and the brecciated interior including many clearly feldspathic (light) clasts and mineral fragments.*

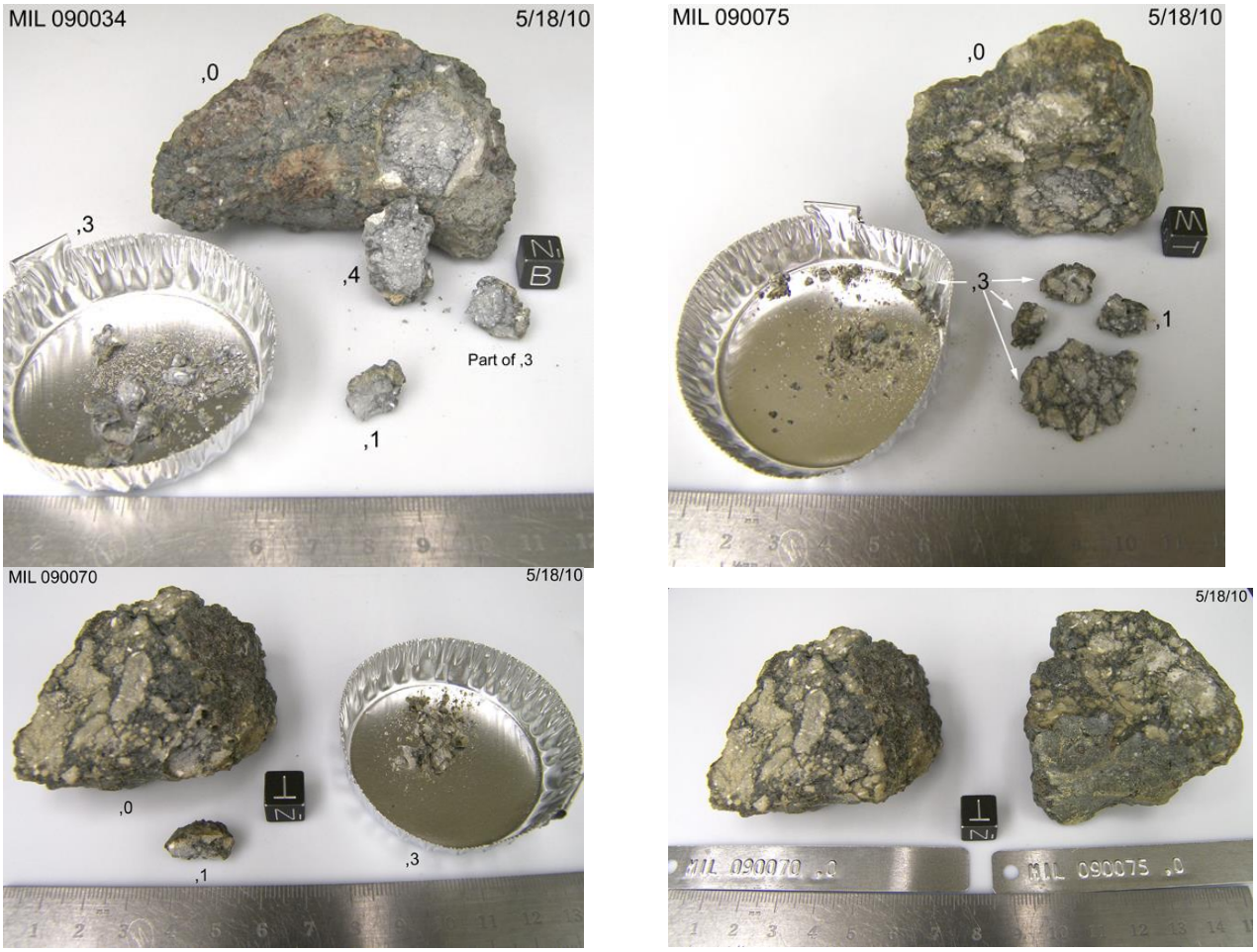

Figure 4: *Macroscopic images of MIL 090034, MIL 090070, and MIL 090075, illustrating the interior textures. Bottom right shows both MIL 090070 and 090075 together before they were broken for characterization.*

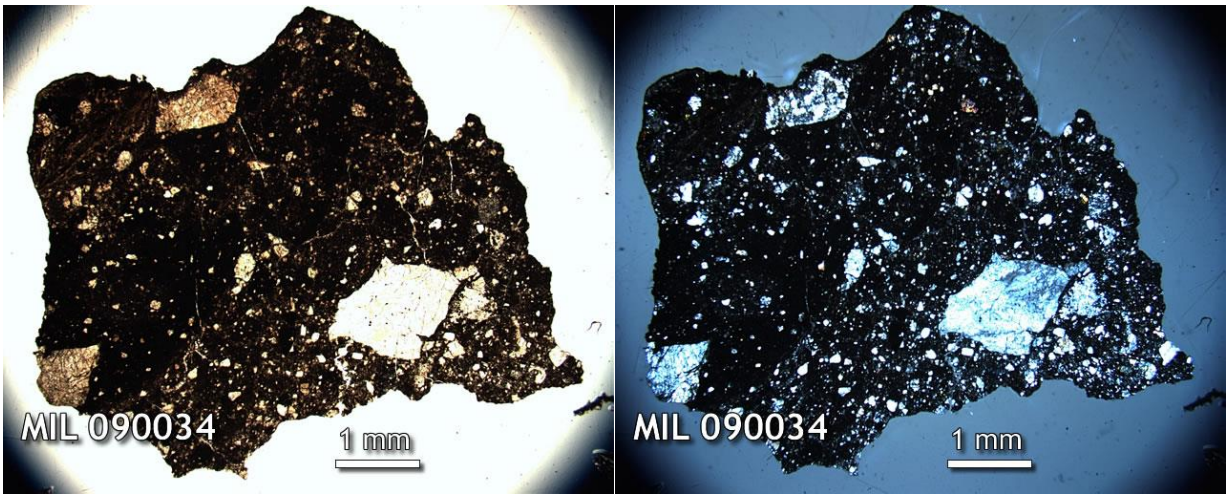

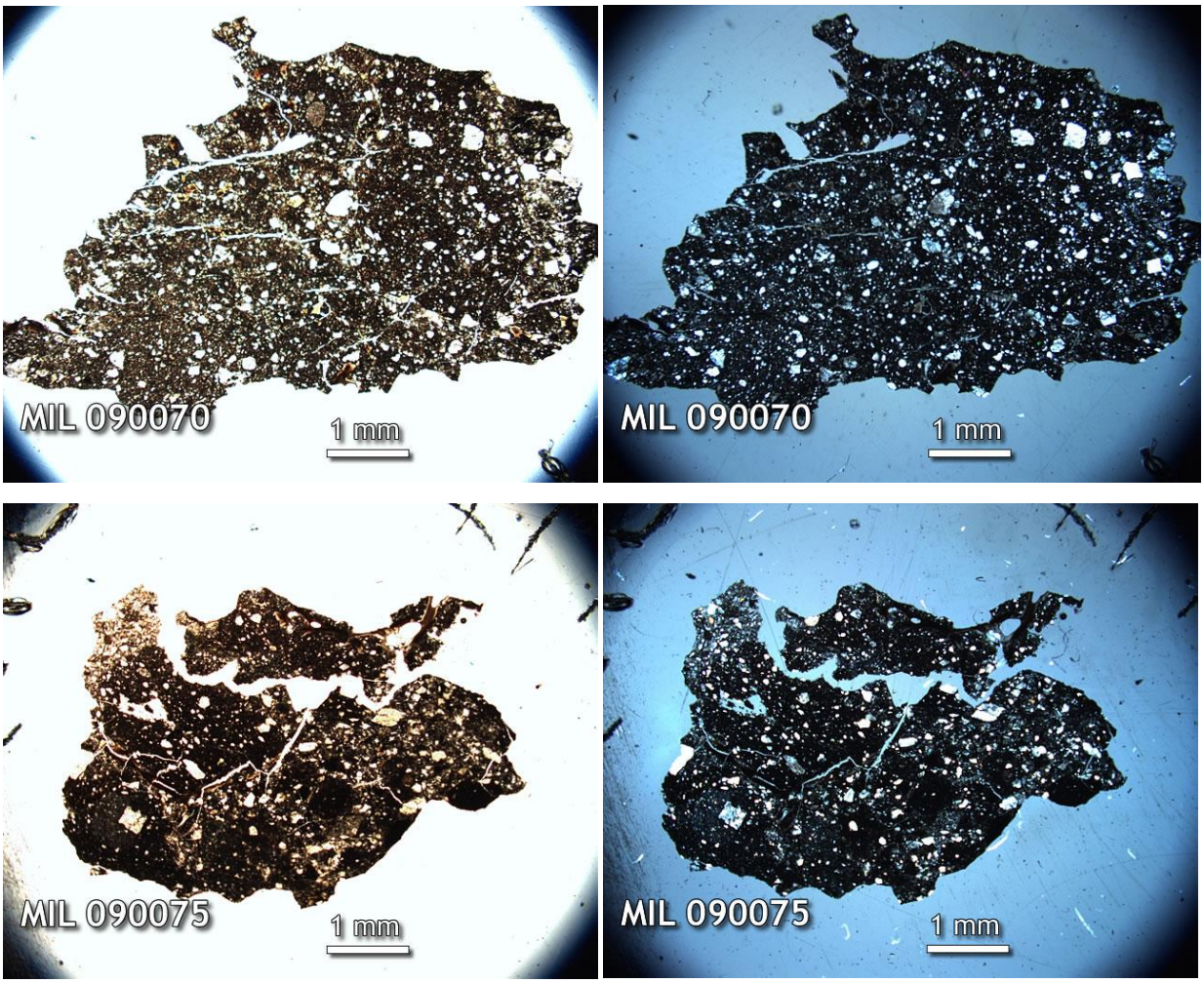

Figure 5: *Microscopic images of MIL 090034, MIL 090070, and MIL 090075, illustrating the brecciated texture. Plane polarized (left) and cross polarized (right) light images of the library section.*

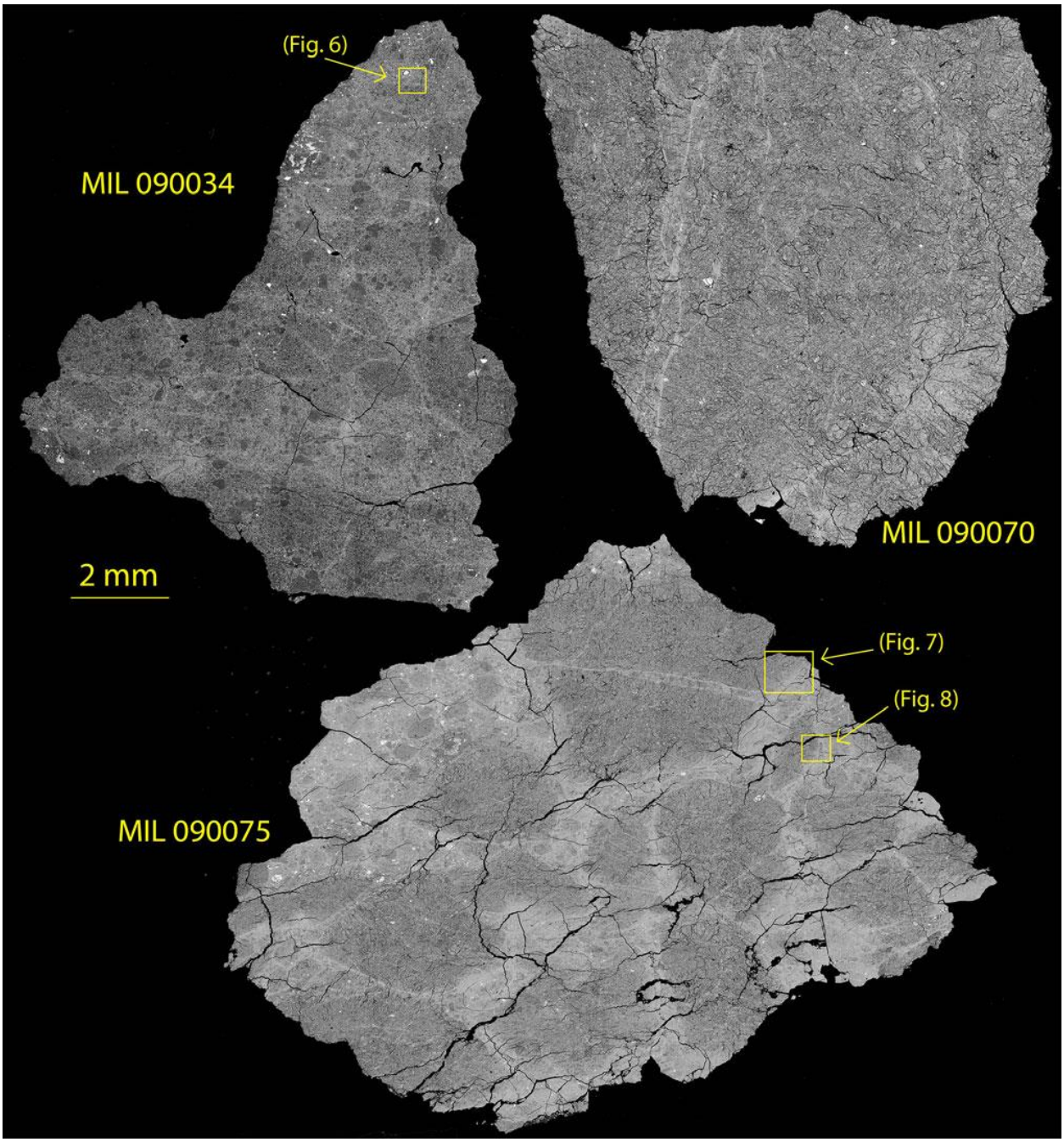

Figure 6: *BSE images of MIL 090034 ,27, MIL 090070 ,25, and MIL 090075 ,21. Clasts outlined in yellow rectangles are from the original reference and the interested reader can look there for more detail (figures from Martin et al., 2017).*

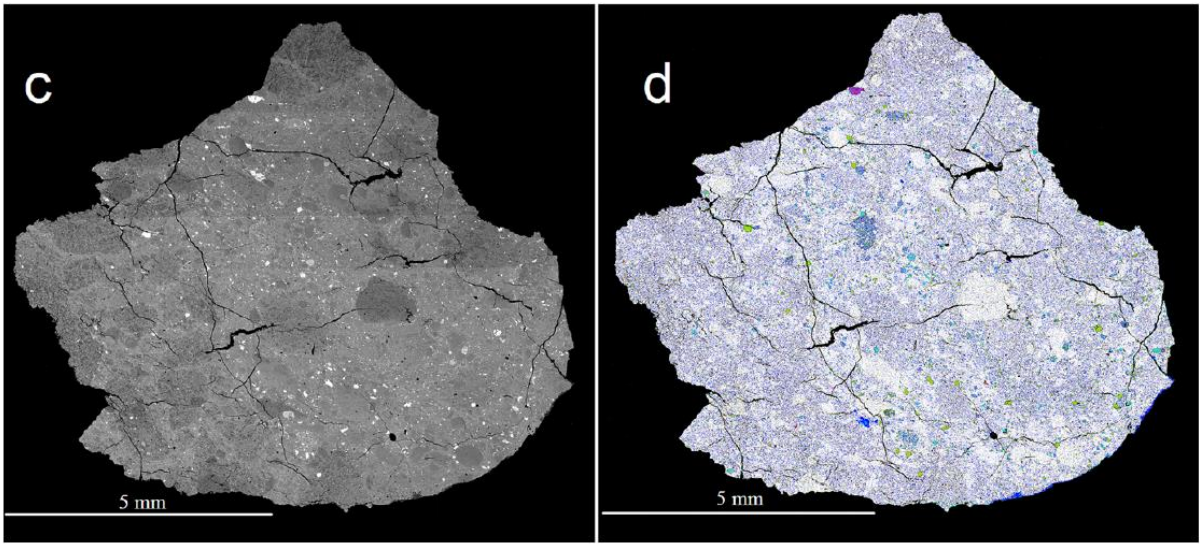

Figure 7: *(a) BSE image of MIL 090070, 35; (b) False-color element map of MIL 090070, 35 showing distribution and qualitative concentration of elements present (from Calzada-Diaz et al. 2016).*

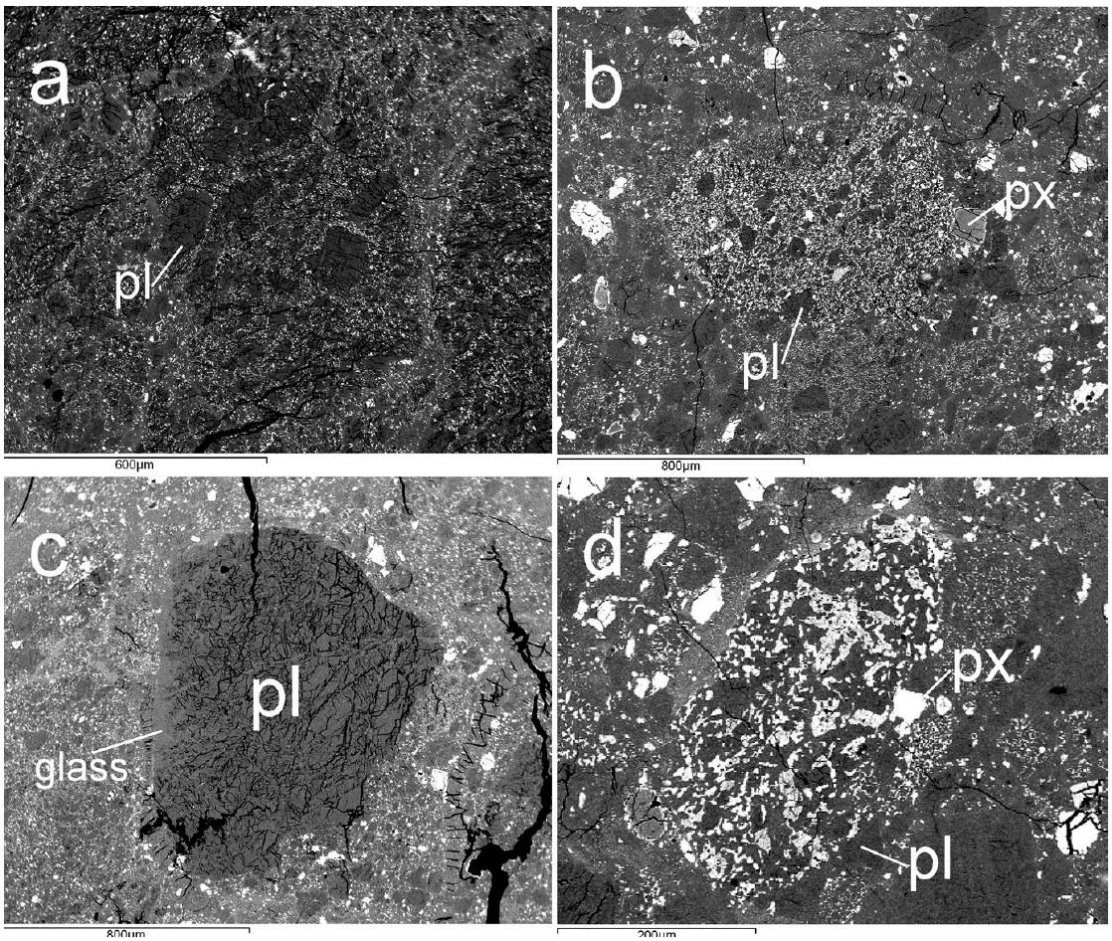

Figure 8*: Backscattered electron images of clasts in MIL 090070 ,35 (figure from Calzada-Diaz et al. 2016).*

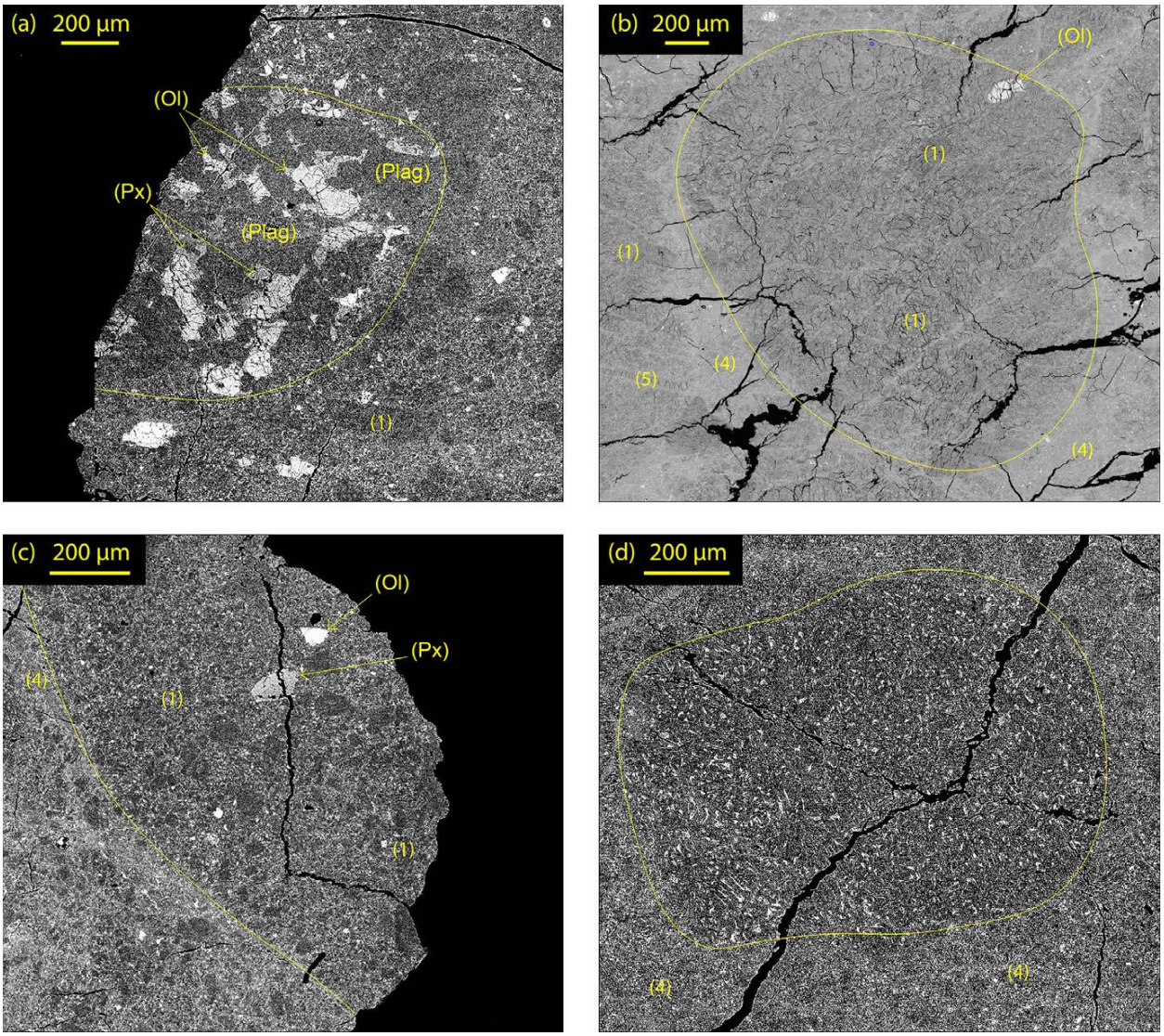

***Figure 9**: Backscattered electron images of clasts in MIL 090034, MIL 090070, and MIL 090075 (figure from Martin et al. 2017). a) Igneous-textured clast. Note the sinuous edges of the olivine (Ol) and pyroxene (Px) crystal fragments within the plagioclase matrix (Plag). b) Typical crystalline anorthite (1) clast-rich impact breccia clast surrounded by polycrystalline impact melt (4). c) A more highly reworked crystalline anorthite (1) clast-bearing impact breccia clast with olivine (Ol) and pyroxene (Px) fragments present. d) Clast-poor impact melt breccia clast surrounded by polycrystalline impact melt (4). Large clasts are highlighted in yellow.*

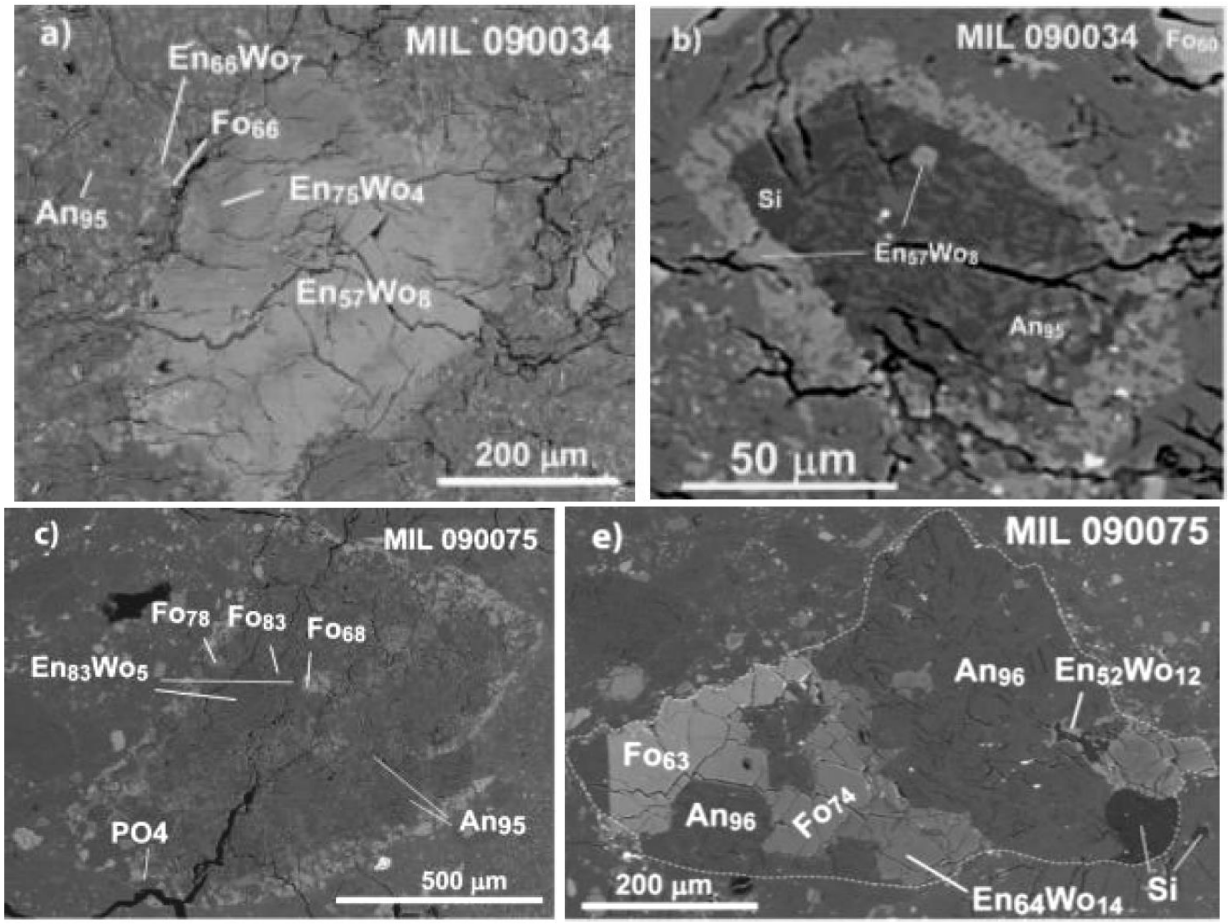

***Figure 10**: Backscattered electron images of clasts and textures in MIL 090034 and MIL 090075 (figure from Liu et al. 2011). A) a large gabbroic clast of 5 mm size in MIL 090034. Here shows the Mg-rich pyroxene. B) A small "granite" clast [cristobalite (Si) + pigeonite + anorthite] enclosed by pigeonite. C) A granulite clast consists of anorthosite (An_{95}), olivine (Fo_{68-83}), and enstatite ($En_{83}Wo_5$). E) A gabbro clast consisting olivine, anorthite, and cristobalite (Si). Note the difference in scales.*

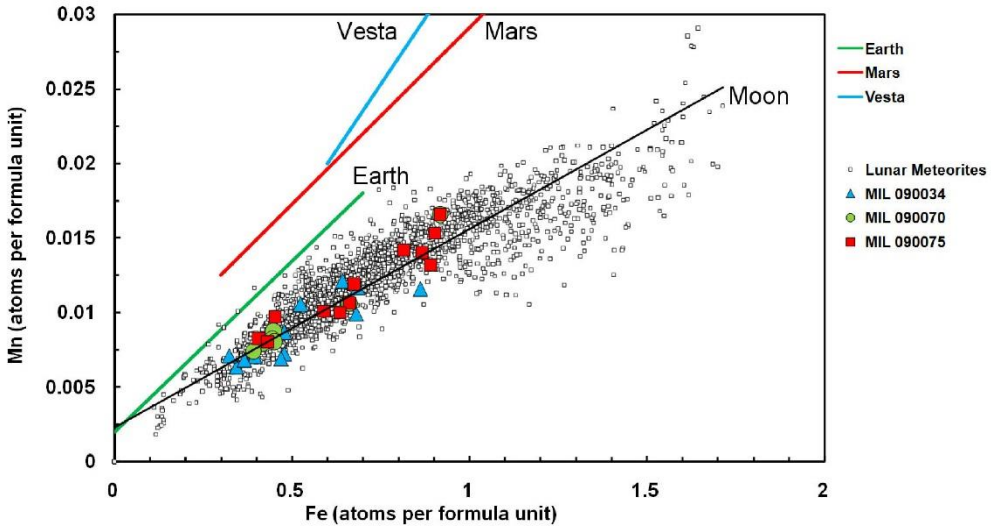

Figure 11: *Fe/Mn ratio of cations in pyroxene crystal fragments in MIL 090034, 090070, and 090075 (figure from Martin et al. 2017).*

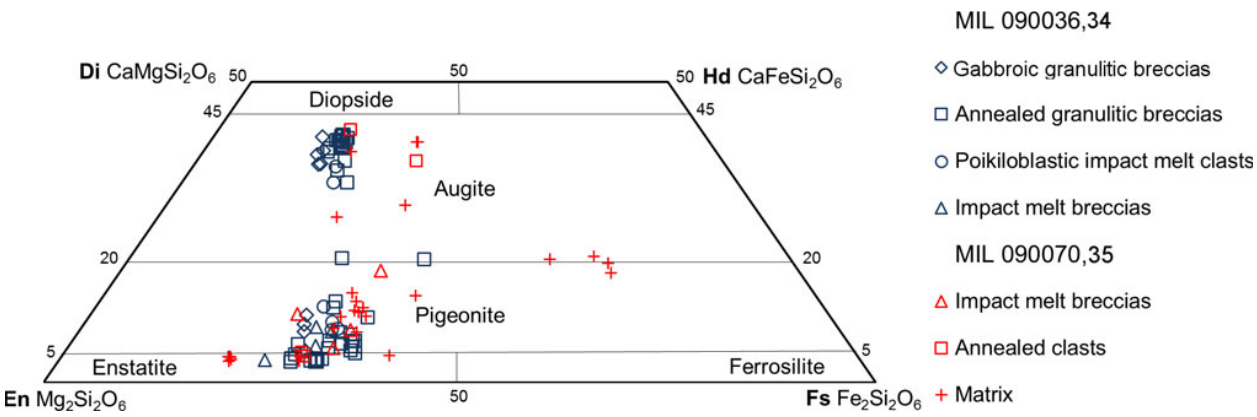

Figure 12: *Pyroxene quadrilateral showing compositions of pyroxenes in various clasts in MIL 090036 compared to MIL 090070 (figures from Calzada-Diaz et al. 2016).*

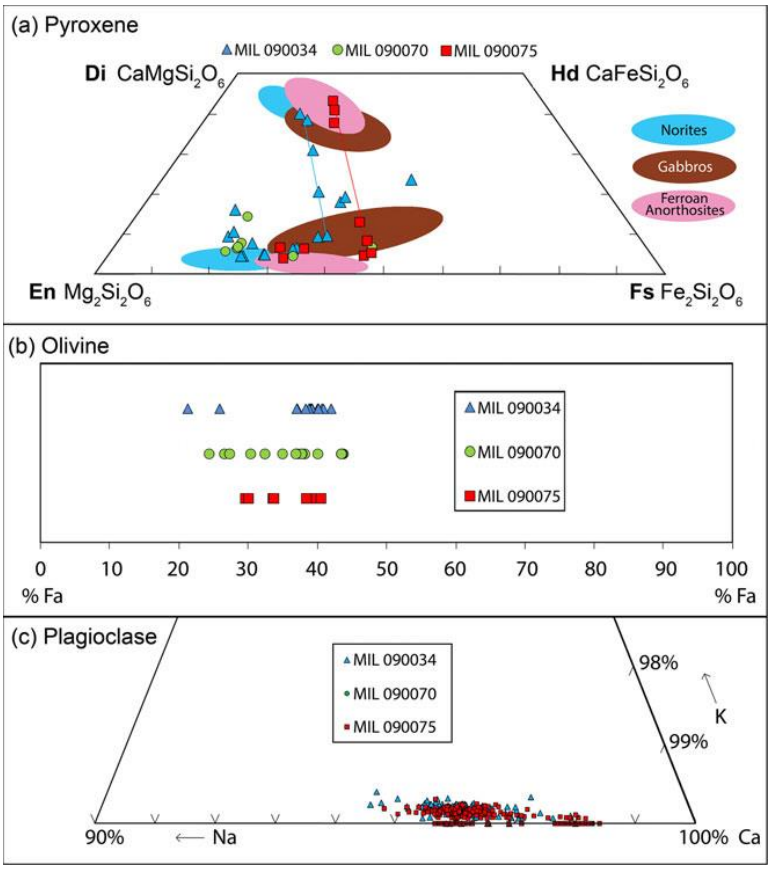

Figure 13: *Pyroxene quadrilateral (top), olivine (middle) and plagioclase (bottom) showing compositions of pyroxenes in various clast (figure from Martin et al. 2017).*

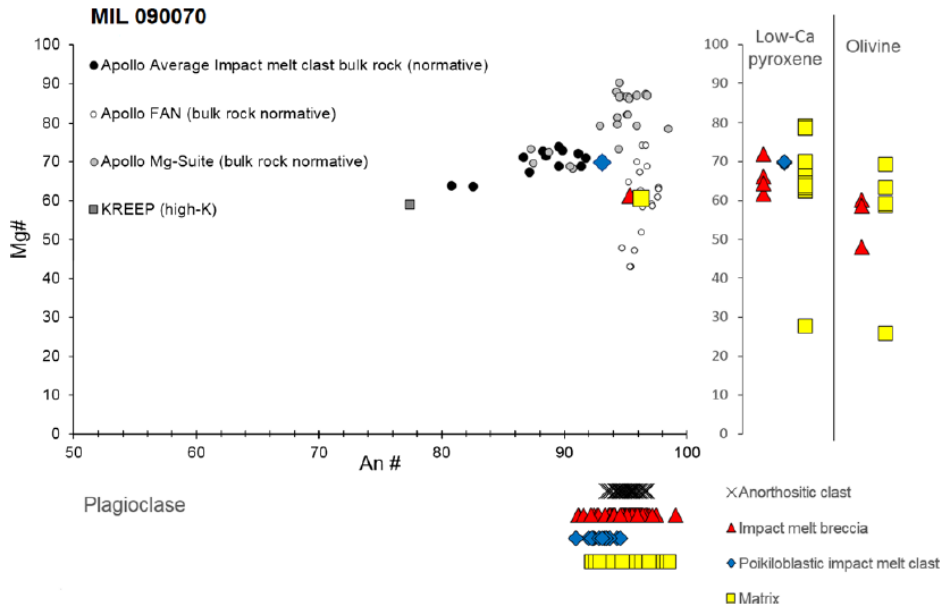

Figure 14: *Mg# of mafic minerals versus An content of plagioclase for clasts in MIL 090070 (top) and compositions of plagioclase grains in MIL 090070 (bottom) (figures from Calzada-Diaz et al. 2016).*

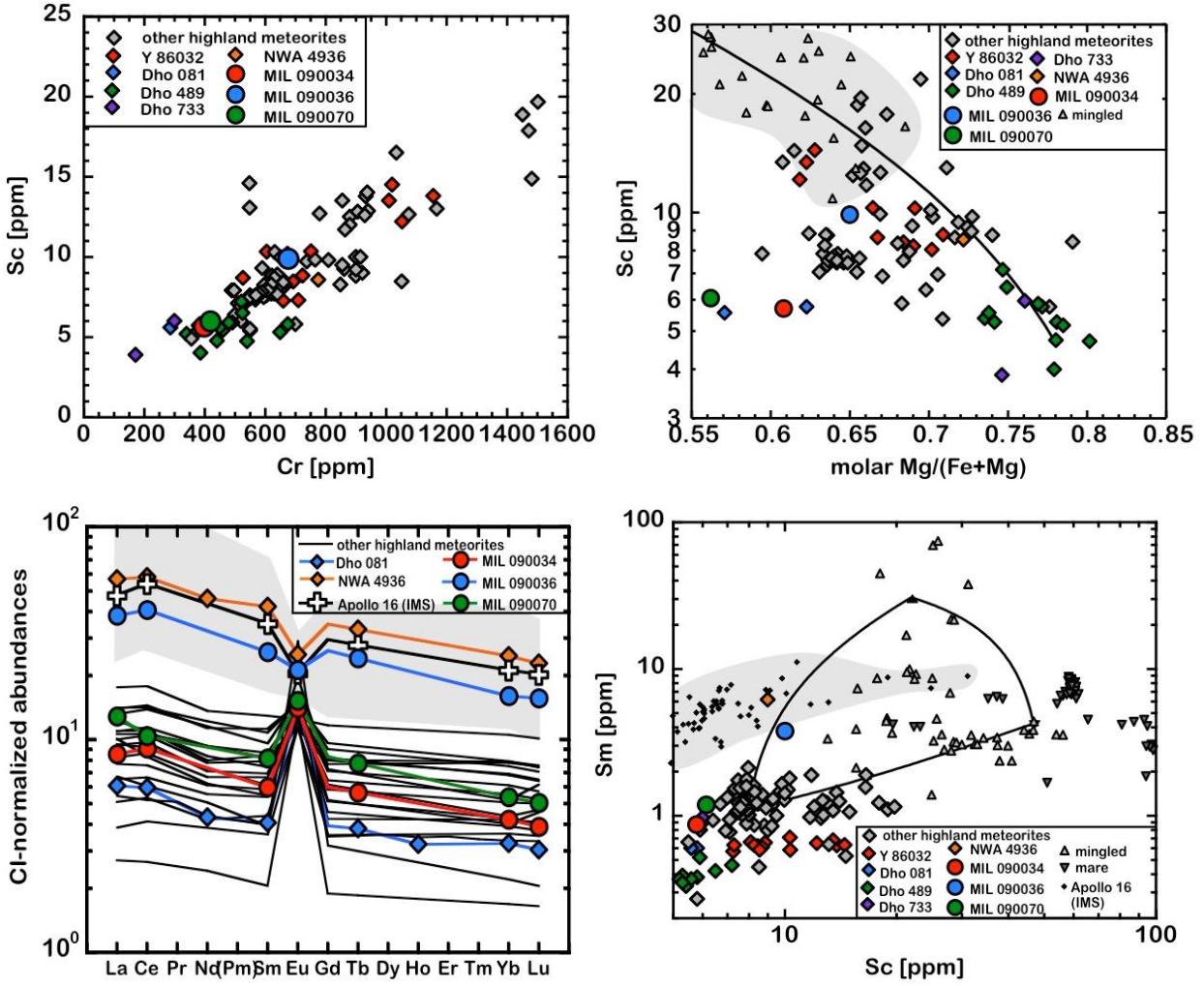

Figure 15*: Upper left: Cr vs. Sc abundances for lunar highland meteorites; upper right: Mg number vs. Sc abundances for lunar highland meteorites. Line represents mixing line of lunar highland meteorites (Dho 489 from Takeda et al., 2006) and mare basalt (Y 793169 from Warren and Kallemeyn, 1993); lower left: CI-normalized rare earth elements abundances for lunar highland meteorites and impact melt splashes from Apollo 16. Light dark shaded regions represent compositional ranges of impact melt splashes from Apollo 16 (Morris et al., 1986); lower right: Sc vs. Sm abundances for lunar highland, mingled and mare meteorites. Lines represent mixing line of FHT, PKT and maria. Data of FHT, PKT and maria, and impact melt splashes from Apollo 16 are taken from Korotev et al. (2009) and Morris et al. (1986) (figures from Shirai et al. 2012).*

Chemistry

MIL 090034, MIL 090070, and MIL 090075 are compositionally similar, and have low Sc, Sm, Cr, and Mg#, but positive Eu anomalies (**Figure 15).** In addition, MIL 090034, MIL 090070, and MIL 090075 have low FeO and very high Al_2O_3 (**Figure 16**). La and Yb contents of these three meteorites all show very negligible KREEP compoenet (**Figure 17)**, and all lower than the minor KREEP component present in MIL 090036, that distinguishes it compositionally from the other MIL 09 lunar breccias (Calzada-Diaz et al., 2016, Xie et al., 2014, Zeigler et al., 2016, Shirai et al., 2012, Liu et al., 2011, Korotev and Ziegler, 2015).

MIL 090034, MIL 090070, and MIL 090075 have been included in a few focused isotopic studies. Ne and Xe isotopes indicate that there are dominant solar wind and fissionogenic components in MIL 090034 and 090070 compared to MIL 090036 (cosmogenic) (**Figure 18**; Park et al., 2019). The potassium isotopic composition of MIL 090070 falls within the range of lunar samples in general and similar to bulk silicate Earth (BSE) potassium, but is distinct from the MIL 090036 lunar breccias (Tian et al., 2020). Finally, the MIL 090034, MIL 090070, and MIL 090075 Os isotopic and HSE concentrations were analyzed as part of a broader study to examine the composition of impactors striking the Moon over time and various locations (McIntosh et al., 2020).

Radiogenic age dating and cosmogenic exposure ages

Reported $^{39}Ar/^{40}Ar$ ages show that the MIL 090034, MIL 090070, and MIL 090075 breccias have ages that are similar to the Imbrium event near 3.9 Ga (summarized in **Fig. 19-22**).

MIL 090034, MIL 090070, and MIL 090075 have young cosmic ray exposure ages of 1-2 Ma whereas MIL 090036 has an older age of ~50±10 Ma (Nishiizumi and Caffee, 2013). ^{37}Ar analyses also indicate an older and distinct age for MIL 090036 compared to the other MIL 09 lunar breccias (MIL 090034, MIL 090070, and MIL 090075), and suggest an origin from shallow subsurface (depths 40-60 cm; **Figure 23**) and a short transit time to Earth (Calzada-Diaz et al., 2016; Nishiizumi and Caffee, 2013; Park et al., 2013).

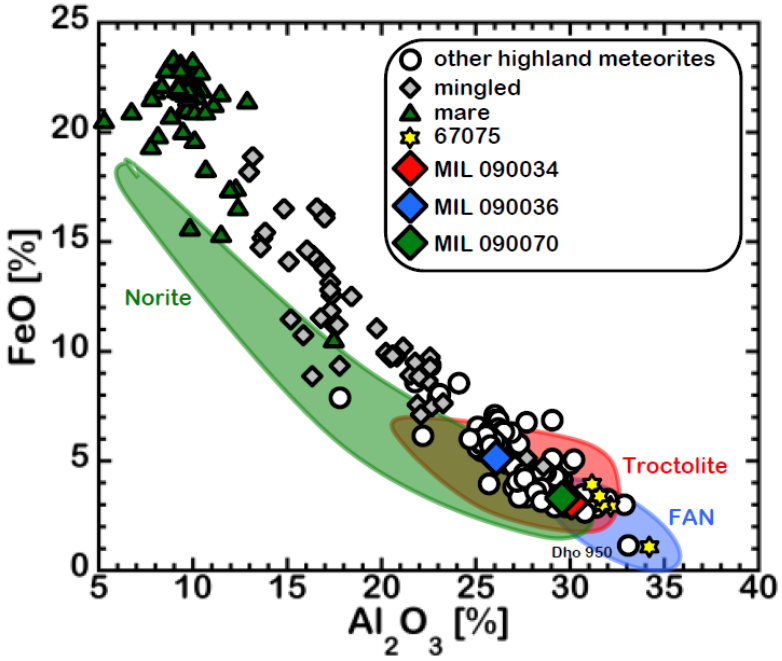

Figure 16: *Although all of the MIL 09 lunar breccias plot within the troctolite field, only MIL 090034 and MIL 090070 fall within the FAN field, this showing the distinctly different composition of MIL 090036 (from Park et al. 2013).*

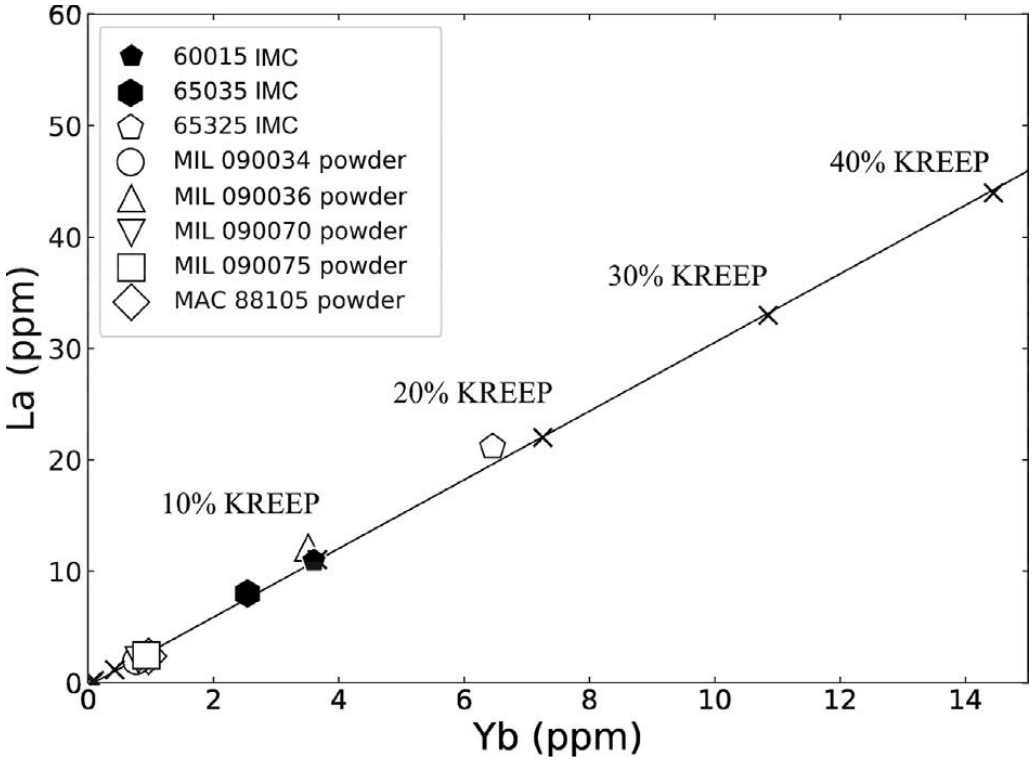

Figure 17: *Demonstration of slightly larger KREEP component present in MIL 090036 (open triangle) and similar to Apollo 16 impact melt clasts, compared to the other MIL 09 lunar breccias, based on La and Yb contents (from McIntosh et al., 2020).*

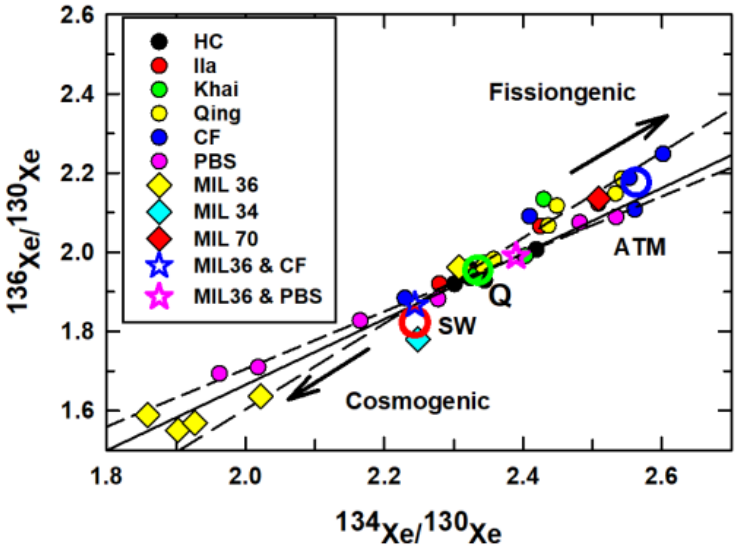

Figure 18*: $^{136}Xe/^{130}Xe$ vs. $^{134}Xe/^{130}Xe$ for lunar and enstatite meteorites near Solar Wind (SW), Q, and terrestrial atmosphere compositions (ATM). HC = Happy Canyon, Ila = Ilafegh, Khai = Khairpur, Qing = Qingzhen, CF = Cumberland Falls, PBS = Peña Blanca Springs. The most cosmogenic data for MIL 090036 and most fissionogenic data for CF are not shown. Intersections for regression lines are shown by open stars color-coded to the corresponding data, trapped compositions by open circles (figure from Park et al., 2019).*

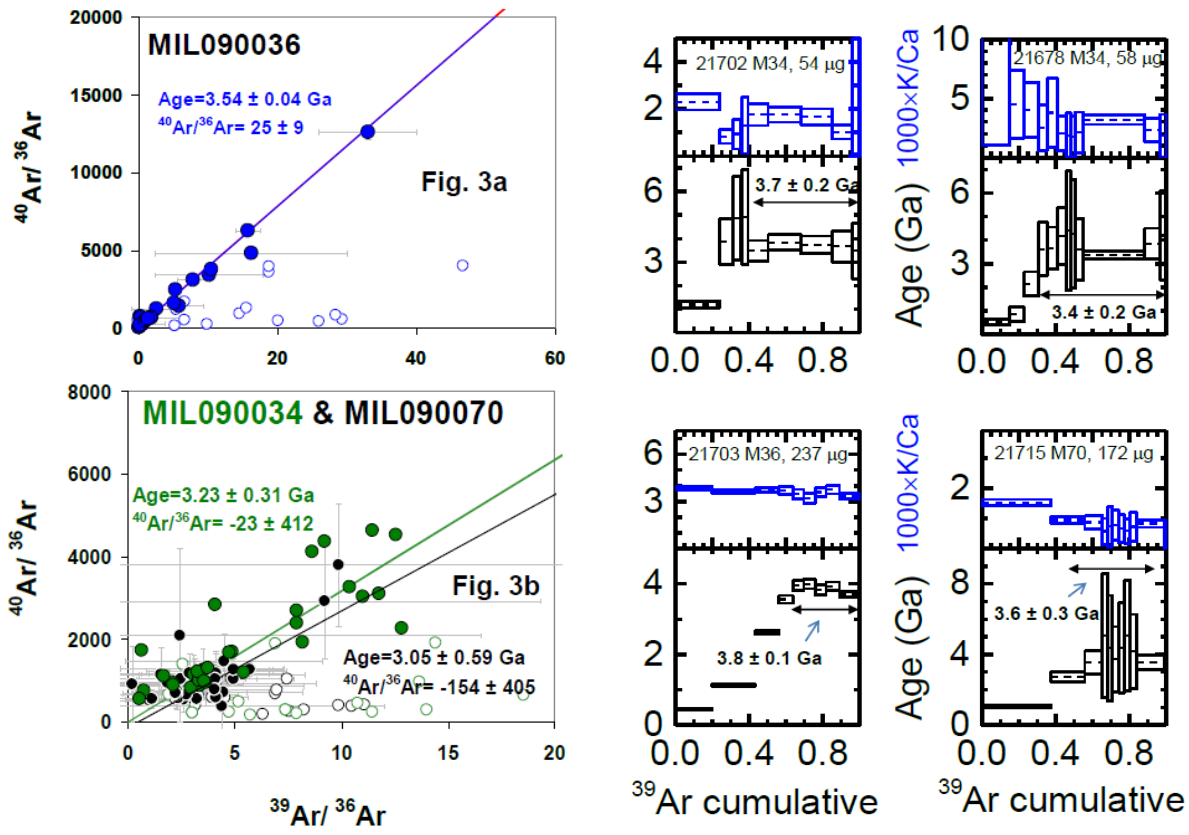

Figure 19: Left: *$^{40}Ar/^{36}Ar$ vs. $^{39}Ar/^{36}Ar$ isochrons for MIL 090036 (a) and MIL 090034 plus MIL 090070 (b). Low temperature data shown by open symbols were excluded from the regressions.* ***Right:*** *Apparent Age spectra and K/Ca ratios of MIL 090034, MIL 090036 and MIL 090070 (figures from Park et al. 2013).*

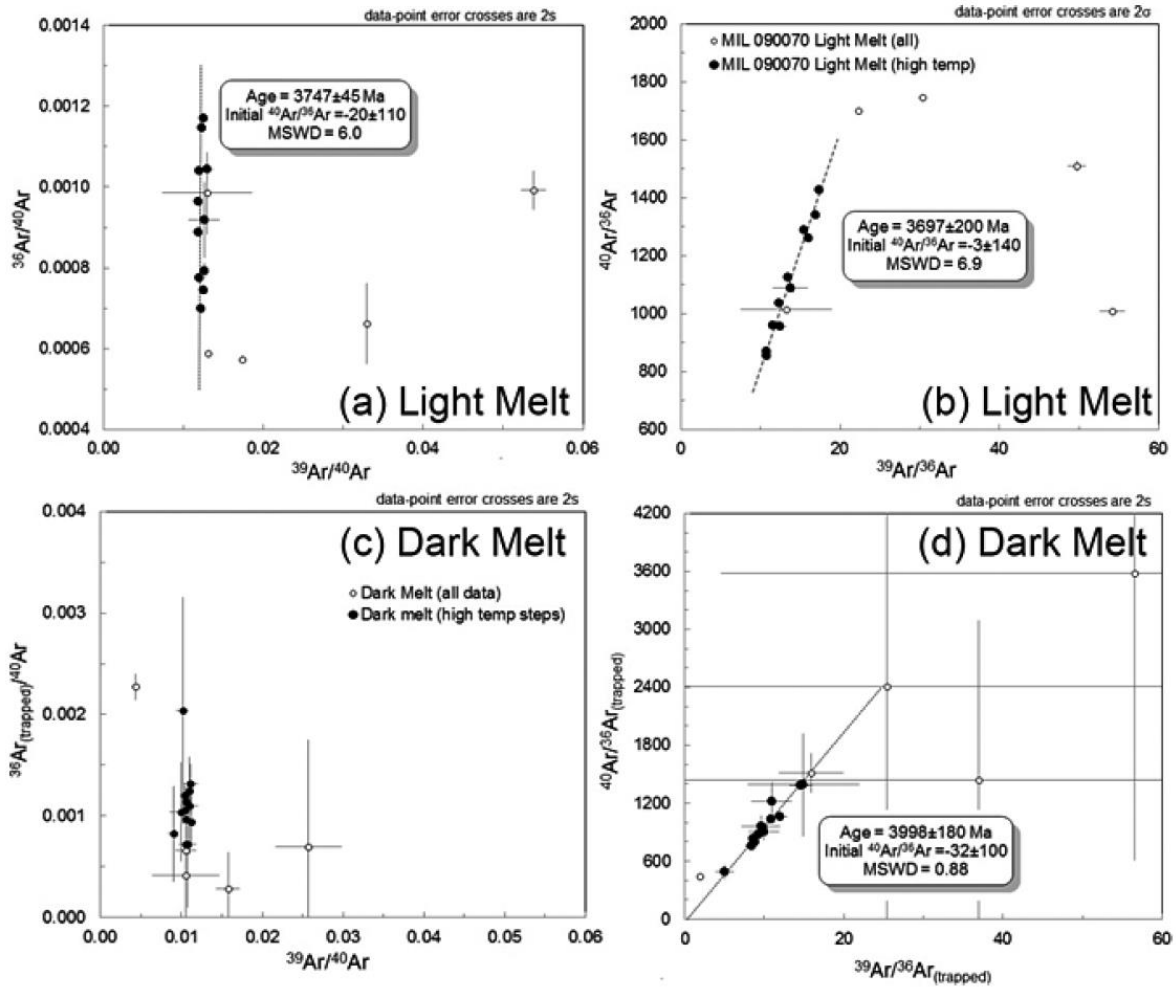

Figure 20: *(a) Inverse argon isotope isochron of $^{39}Ar/^{40}Ar$ versus $^{36}Ar/^{40}Ar$ ratios and (b) normal argon isotope isochron of $^{39}Ar/^{36}Ar$ versus $^{40}Ar/^{36}Ar$ ratios for MIL 090070,33 Light Melt Clast. (c) Inverse argon isotope isochron of $^{39}Ar/^{40}Ar$ versus $^{36}Ar/^{40}Ar$; (d) and normal argon isotope isochron of $^{39}Ar/^{36}Ar$ versus $^{40}Ar/^{36}Ar$ for MIL 090070,33 Dark Melt component. ^{36}Ar(trapped) refers to ^{36}Ar corrected for cosmogenic contribution. Dashed line is a fit to bulk sample high temp steps (excluding final step), giving model isochron ages and initial $^{40}Ar/^{36}Ar$ ratios. Calculated isochron ages are not significant as data cluster at the radiogenic component (figure from Calzada-Diaz et al. 2016).*

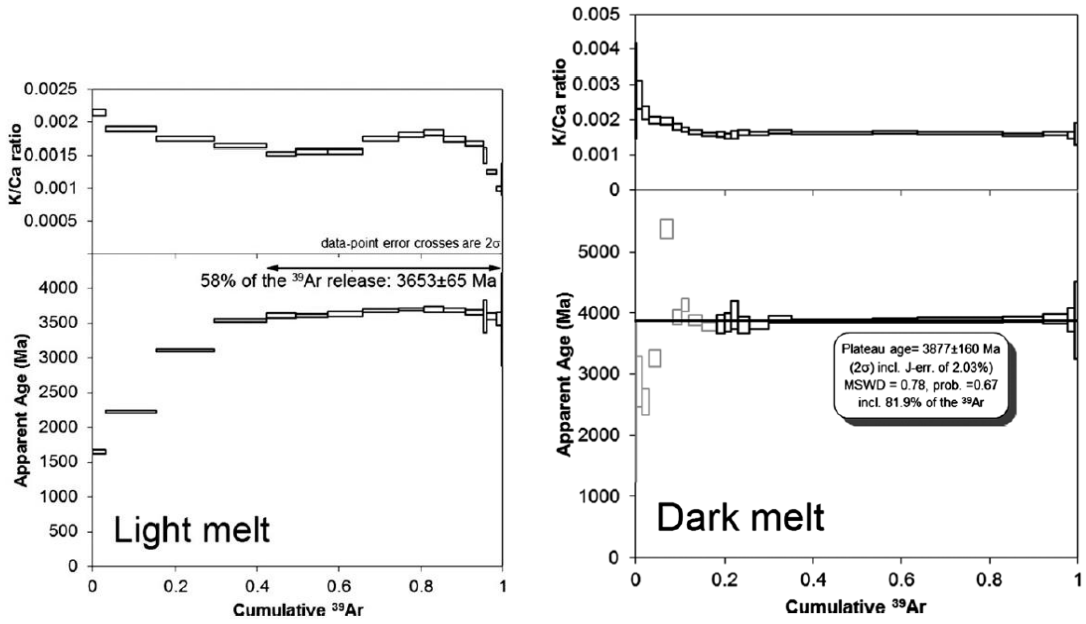

***Figure 21: Left**: Model age argon release profiles for the light melt component in MIL 090070. Top panel shows K/Ca mole values derived from $^{39}Ar/^{37}Ar$ ratio released at each temperature step versus cumulative % of ^{39}Ar released from each step-heating. This is compared in the lower panels with the apparent ^{40}Ar-^{39}Ar age spectra where each box represents a single step release including a 2σ error. The age shown is a part fusion release age from 58% of the ^{39}Ar release. **Right**: Model age argon release profiles for the dark melt component in MIL 090070. Top panel show K/Ca mole values derived from $^{39}Ar/^{37}Ar$ ratio released at each temperature step versus cumulative% of ^{39}Ar released from each step-heating. This is compared in the lower panels with the apparent ^{40}Ar-^{39}Ar age spectra where each box represents a single step release including a 2σ error. Gray boxes represent those that are not included in the plateau age calculation. Plateau age reported includes external error on the monitor age. (figure from Calzada-Diaz et al. 2016).*

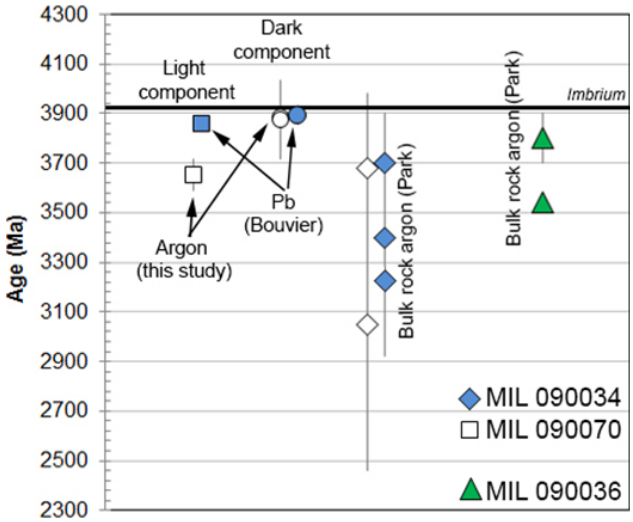

***Figure 22:** Summary of events recorded by Ar and Pb isotopes for components and bulk-rock samples of MIL 090034 (Bouvier et al. 2013; Park et al. 2013), MIL 090070 (Park et al. 2013; Bouvier et al. 2013; and Calzada-Diaz et al. 2016). Park et al. (2013) determined argon isotope plateau and normal isochron age models. Bouvier et al. (2013) report Pb isotopes. The data from Calzada-Diaz et al. 2016 reflect argon fusion ages and a plateau age. Age of the Imbrium basin-forming event is shown for reference using the reported age of Snape et al. (2015) of 3915 Ma (figure from Calzada-Diaz et al. 2016).*

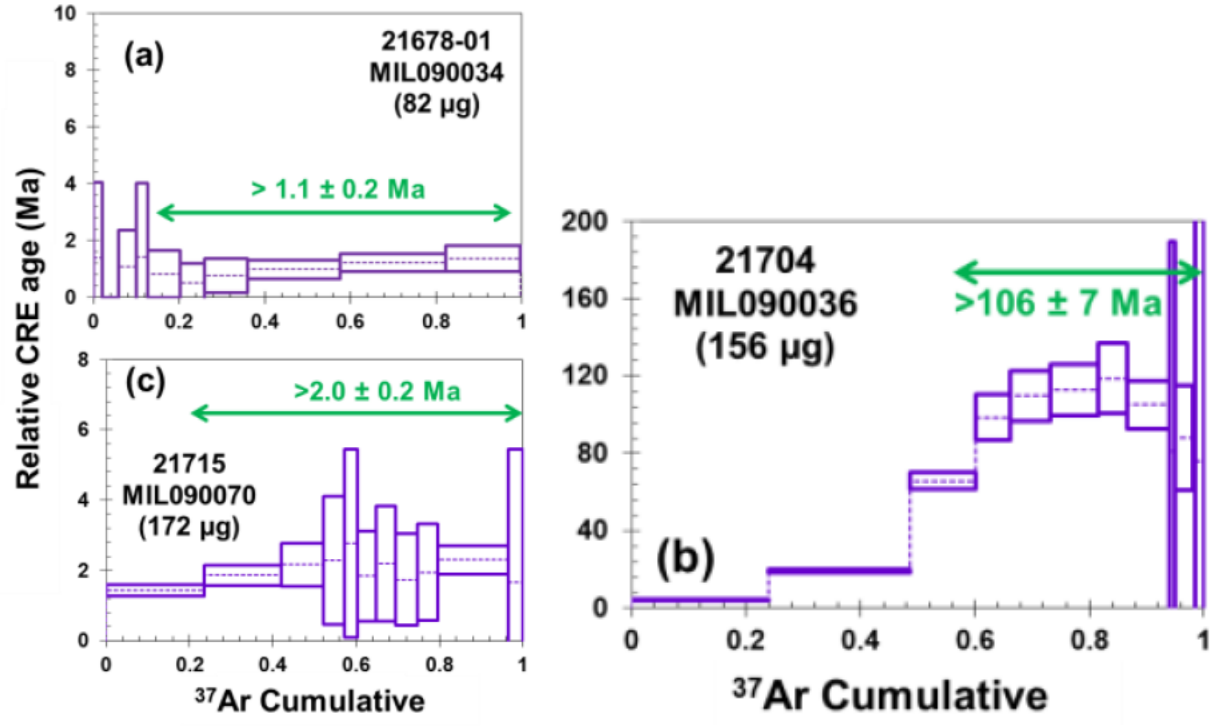

Figure 23: *Lower bounds on the relative CRE ages (values above arrows) differentiate MIL 090034, and MIL 090070 from MIL 090036 (figures from Park et al. 2013).*

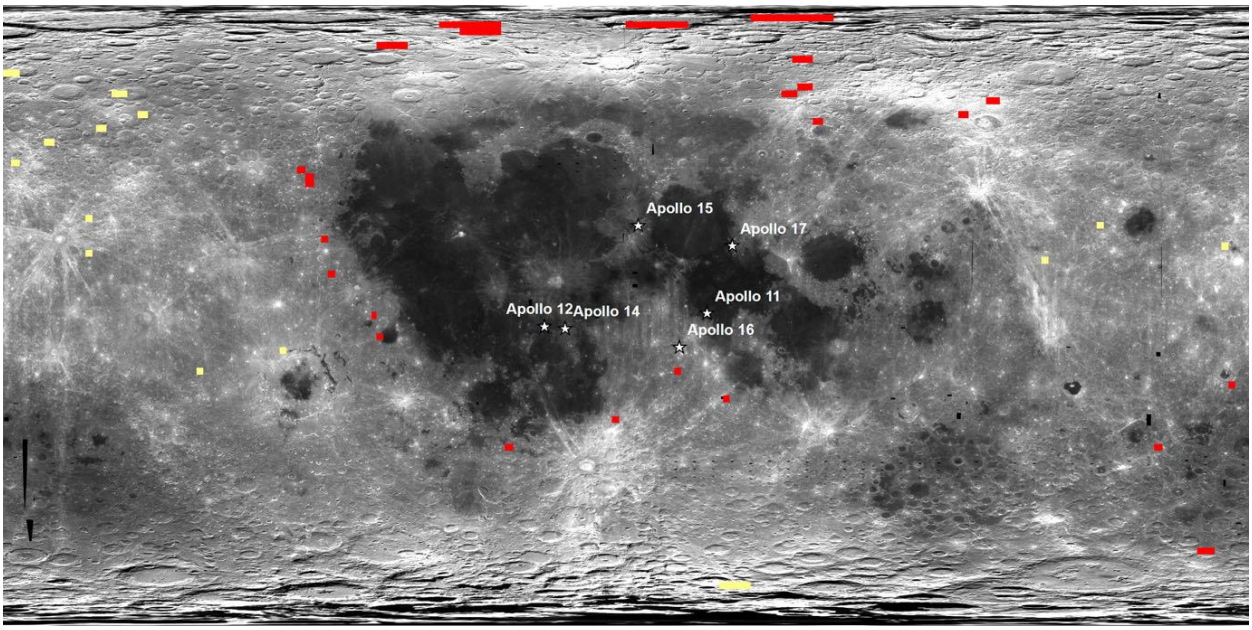

Figure 24*: Image showing the areas where surface regolith FeO, TiO_2, and Th composition measurements obtained by Lunar Prospector Gamma Ray Spectrometer (Prettyman et al. 2006) match the analytical composition of regolith breccias MIL 090036 in red and MIL 090070 and paired stones MIL 090034 and MIL 090075 (Korotev and Zeigler 2015) in yellow (Table 2). Underlying albedo image of the Moon is a Clementine albedo map in a cylindrical projection with 0° longitude in the center (from Calzada-Diaz et al. 2016).*

Summary

Studies of the mineralogy, petrology, and geochemistry of MIL 090034, 090070, and 090075 have shown that they are a mixture of different feldspathic lithologies including impact melt breccias, noritic and gabbroic clasts, and plagioclase and pyroxene mineral clasts and fragments. MIL 090034, 090070, and 090075 are compositionally and isotopically distinct (very high Al_2O_3 and low FeO) from the MIL 090036 lunar breccia. It has a negligible KREEP component, no evidence for significant mare/basaltic lithologies, and many clasts are compositionally similar to ferroan anorthosite (FAN) lithologies that are present in Apollo 16 materials. Comparison of bulk FeO, TiO_2, and Th in MIL 090034, 090070, and 090075 to global lunar geochemical data shows a likely origin in the farside highlands, but a south polar region cannot be ruled out (**Fig. 24**).

Splits of MIL 090034 as of January 2024 (not including attrition)

split	mass (g)	parent	form	PI-1	PI-2	current
0	143.57	-	DOC PC	-	-	JSC
1	1.138	0	PB	-	-	JSC
2	0.01	1	TS	SI	-	SI
3	3.298	0	CPS+FI	-	-	JSC
4	6.462	0	DOC CP	-	-	JSC
6	0.01	1	TS	Treiman	-	Treiman
7	0.01	1	TS	Trigo	-	Trigo
8	0.01	1	THK	Liu	-	Liu
9	0.01	1	TS	Gross	-	Gross
10	0.01	1	TS	Liu	-	Liu
11	0.01	1	THK	-	-	JSC
12	0.381	0	INT CPS	Nishiizumi	-	Nishiizumi
13	0.396	0	EXT CPS	Nishiizumi	-	Nishiizumi
14	0.145	0	CPS	Korotev	-	JSC
15	0.801	0	INT CPS	-	-	JSC
16	7.171	0	CPS+FI	-	-	JSC
17	0.414	0	CPS+FI	-	-	JSC
18	0.273	0	EXT CPS	Nishiizumi	-	Nishiizumi
19	0.19	0	CPS	Korotev	-	JSC
20	2.494	0	IN CPS	Yamaguchi	-	Yamaguchi
21	0.786	0	PB	-	-	JSC
22	2.061	0	INT CPS	Liu	-	Liu
23	0.185	0	CPS	Korotev	-	JSC
24	21.3	0	CPS+FI	Britt	-	JSC
26	0.01	21	TS	Yamaguchi	-	Yamaguchi
27	0.01	21	THK	Joy	-	JSC
28	0.01	21	TS	Joy	-	JSC
29	0.652	24	PB	-	-	JSC
31	0.01	29	TS	Zeigler	-	Zeigler

32	0.05	24	IN CP	Joy	Curran	Curran
34	0.21	24	CPS	Bouvier	-	consumed
36	0.58	0	CPS	Bouvier	-	consumed
37	2.04	0	CPS+FI	-	-	JSC
39	0.148	15	CPS	Sehlke	-	Sehlke

Splits of MIL 090070 as of January 2024 (not including attrition)

split	mass (g)	parent	form	PI-1	PI-2	current
0	74.707	-	DOC PC	-	-	JSC
1	1.609	0	PB	-	-	JSC
2	0.01	1	TS	SI	-	SI
3	0.746	0	CPS+FI	-	-	JSC
6	0.01	1	TS	JSC	-	JSC
7	0.01	1	TS	Korotev	-	JSC
8	0.01	1	THK	Liu	-	Liu
9	0.01	1	TS	Liu	-	Liu
10	0.01	1	TS	JSC	-	JSC
11	0.01	1	TS	Miao	-	JSC
12	0.289	0	EXT CPS	Nishiizumi	-	Nishiizumi
13	0.112	0	CPS	Korotev	-	JSC
14	0.345	0	INT CPS	Nishiizumi	-	Nishiizumi
15	2.13	0	INT CPS	Liu	-	Liu
16	0.167	0	CPS	Korotev	-	JSC
17	2.543	0	INT CPS	Yamaguchi	-	Yamaguchi
18	1.075	0	PB	-	-	JSC
19	8.666	0	LOC CP	Britt	-	JSC
20	0.235	0	CPS	Korotev	-	JSC
21	0.329	0	EXT CPS	Nishiizumi	-	Nishiizumi
22	21.32	0	CPS+FI	-	-	JSC
24	0.01	18	TS	Yamaguchi	-	Yamaguchi
25	0.01	18	THK	Joy	-	JSC
26	0.01	18	TS	Joy	-	JSC
27	0.438	22	PB	-	-	JSC
29	0.01	27	TS	Zeigler	-	Zeigler
30	0.05	22	IN CP	Joy	Curran	Curran
32	1.92	19	CP	-	-	JSC
33	0.275	22	INT CPS	Crawford	-	consumed
35	0.01	27	TS	Crawford	-	Crawford
36	0.3	22	INT CP	Wang	-	consumed
38	2.249	22	INT CPS	Kruijer	-	Kruijer
39	0.178	0	INT CP	Sehlke	-	Sehlke
40	17.243	0	CPS+FI	-	-	JSC

Splits of MIL 090075 as of January 2024 (not including attrition)

split	mass (g)	parent	form	PI-1	PI-2	current
0	117.963		DOC PC	-	-	JSC
1	0.917	0	PB	-	-	JSC
2	0.01	1	TS	SI	-	SI
3	5.533	0	CPS+FI	-	-	JSC
5	0.01	1	TS	JSC	-	JSC
6	0.01	1	TS	Korotev	-	JSC
7	0.01	1	THK	Liu	-	Liu
8	0.01	1	TS	Liu	-	Liu
9	0.01	1	THK	JSC	-	JSC
11	0.193	0	CPS	Korotev	-	JSC
12	0.334	0	EXT CPS	Nishiizumi	-	Nishiizumi
13	0.341	0	INT CPS	Nishiizumi	-	Nishiizumi
14	0.125	0	CPS	Korotev	-	JSC
15	2.008	0	INT CPS	Liu	-	Liu
16	1.701	0	PB	-	-	JSC
17	0.199	0	CPS	Korotev	-	JSC
18	0.328	0	INT CP	Nishiizumi	-	Nishiizumi
19	12.88	0	CPS+FI	-	-	JSC
21	0.01	16	THK	Joy	-	JSC
22	0.01	16	TS	Joy	-	JSC
23	0.488	19	PB	-	-	JSC
25	0.01	23	TS	Zeigler	-	Zeigler
26	0.09	19	IN CP	Joy	Curran	Curran
28	0.165	3	INT CPS	Sehlke	-	Sehlke

References:

Calzada-Diaz, A., Joy, K. H., Crawford, I. A., & Strekopytov, S. (2017) The petrology, geochemistry, and age of lunar regolith breccias Miller Range 090036 and 090070: Insights into the crustal history of the Moon. . Meteoritics & Planetary Science, 52, 3-23, doi: 10.1111/maps.12737.

Korotev, R.L., and Zeigler, R.A. (2015) ANSMET Meteorites from the Moon. In Righter, K., Corrigan, C.M., McCoy, T.J., and Harvey, R.P. *Meteorites: A Pictorial Guide to the Collection*, First Edition, AGU Wiley, pp. 101-130.

Liu, Y., Patchen, A., & Taylor, L. A. (2011) Lunar highland breccias MIL 090034/36/70/75: A significant KREEP component. In *42nd Annual Lunar and Planetary Science Conference* (No. 1608, p. 1261).

Martin, D. J., Pernet-Fisher, J. F., Joy, K. H., Wogelius, R. A., Morlok, A., & Hiesinger, H. (2017) Investigating the shock histories of lunar meteorites Miller Range 090034, 090070, and 090075 using petrography, geochemistry, and micro-FTIR spectroscopy. . Meteoritics & Planetary Science, 52, 1103-1124, doi: 10.1111/maps.12860.

McIntosh, E. C., Day, J. M. D., Lui, Y., Jiskoot, C. (2020) Examining the compositions of impactors striking the Moon using Apollo impact melt coats and anorthositic regolith breccia meteorites. Geochimica et Cosmochimica Acta, 274, 192-210, doi: 10.1016/j.gca.2020.01.051.

Nishiizumi, K., & Caffee, M. W. (2013) Relationships among six lunar meteorites from Miller Range, Antarctica based on cosmogenic radionuclides. In *44th Annual Lunar and Planetary Science Conference* (No. 1719, p. 2715).

Park, J., Nyquist, L. E., Shih, C. Y., Herzog, G. F., Yamaguchi, A., Shirai, N., ... & Swisher, C. C. (2013) Late Bombardment of the Lunar Highlands Recordeded in MIL 090034, MIL 090036 and MIL 090070 Lunar Meteorites. In *44th Annual Lunar and Planetary Science Conference* (No. 1719, p. 2576).

Park, J., Nagao, K., Nyquist, L.E., Herzog, G.F., Choi, J., Baek, J.M., Park, C., Lee, J.I., Lee, M.J., Weisberg, M.K. and Ebel, D.S. (2019) Noble Gas Studies of Lunar and Enstatite Meteorites. In *50th Annual Lunar and Planetary Science Conference* (No. 2132, p. 2272).

Satterwhite, C. E. and Righter, K. (2010) Ant. Met. Newsl. 33 no. 2.

Shirai, N., Ebihara, M., Sekimoto, S., Yamaguchi, A., Nyquist, L., Shih, C.Y., Park, J. and Nagao, K. (2012) Geochemistry of Lunar Highland Meteorites MIL 090034, 090036 and 090070. In *43rd Annual Lunar and Planetary Science Conference* (No. 1659, p. 2003).

Tian, Z., Jolliff, B.L., Korotev, R.L., Fegley, B., Lodders, K., Day, J.M.D., Chen, H., Wang, K. (2020) Potassium isotopic composition of the moon. Geochimica et Cosmochimica Acta, 280, 263-280, doi: 10.1016/j.gca.2020.04.021.

Xie, L., Chen, H., Miao, B., Xia, Z., and Yao, J. (2014) Petrography and mineralogy of new lunar meteorite MIL090036. *Advances in Polar Science 25*, 17-25.

Zeigler, R. A., & Korotev, R. L. (2016) Petrography and Geochemistry of Lunar Meteorite Miller Range 13317. In *47th Annual Lunar and Planetary Science Conference* (No. 1903, p. 2554).

Kevin Righter, April 2024